



1 **Examination of Brown Carbon Absorption from Wildfires in the Western U.S. During the**  
2 **WE-CAN Study**

3  
4  
5 Amy P. Sullivan<sup>1</sup>, Rudra P. Pokhrel<sup>2\*</sup>, Yingjie Shen<sup>2</sup>, Shane M. Murphy<sup>2</sup>, Darin W. Toohey<sup>3</sup>,  
6 Teresa Campos<sup>4</sup>, Jakob Lindaas<sup>1</sup>, Emily V. Fischer<sup>1</sup>, and Jeffrey L. Collett, Jr.<sup>1</sup>

7  
8  
9 <sup>1</sup>Colorado State University, Department of Atmospheric Science, Fort Collins, Colorado 80523

10 <sup>2</sup>University of Wyoming, Department of Atmospheric Science, Laramie, WY 82071

11 <sup>3</sup>University of Colorado – Boulder, Department of Atmospheric and Oceanic Sciences, Boulder,  
12 CO 80309

13 <sup>4</sup>National Center for Atmospheric Research, Atmospheric Chemistry Division, Boulder, CO

14 \*now at Cooperative Institute for Research in Environmental Sciences, University of Colorado,  
15 Boulder, CO 80309 and NOAA Chemical Science Laboratory, Boulder, CO 80305

16  
17 Corresponding author: Amy P. Sullivan, [sullivan@atmos.colostate.edu](mailto:sullivan@atmos.colostate.edu)  
18  
19  
20  
21  
22  
23  
24  
25  
26  
27  
28  
29  
30  
31  
32  
33  
34  
35  
36  
37  
38  
39  
40  
41  
42  
43  
44  
45  
46



47 **Abstract**

48 Light absorbing organic carbon, or brown carbon (BrC), can be a significant contributor  
49 to the visible light absorption budget. However, the sources of BrC and the contributions of BrC  
50 to light absorption are not well understood. Biomass burning is thought to be a major source of  
51 BrC. Therefore, as part of the WE-CAN (Western Wildfire Experiment for Cloud Chemistry,  
52 Aerosol Absorption and Nitrogen) Study BrC absorption data was collected aboard the  
53 NSF/NCAR C-130 aircraft as it intercepted smoke from wildfires in the Western U.S. in July-  
54 August 2018. BrC absorption measurements were obtained in near real-time using two  
55 techniques. The first coupled a Particle-into-Liquid Sampler (PILS) with a Liquid Waveguide  
56 Capillary Cell and a Total Organic Carbon analyzer for measurements of water-soluble BrC  
57 absorption and WSOC (water-soluble organic carbon). The second employed a custom-built  
58 Photoacoustic Aerosol Absorption Spectrometer (PAS) to measure total absorption at 405 and  
59 660 nm. The PAS BrC absorption at 405 nm (PAS total Abs 405 BrC) was calculated by  
60 assuming the absorption determined by the PAS at 660 nm was equivalent to the black carbon  
61 (BC) absorption and the BC aerosol absorption Ångström exponent was 1. Data from the PILS  
62 and PAS were combined to investigate the water-soluble vs. total BrC absorption at 405 nm in  
63 the various wildfire plumes sampled during WE-CAN. WSOC, PILS water-soluble Abs 405,  
64 and PAS total Abs 405 tracked each other in and out of the smoke plumes. BrC absorption was  
65 correlated with WSOC ( $R^2$  value for PAS = 0.42 and PILS = 0.60) and CO (carbon monoxide)  
66 ( $R^2$  value for PAS = 0.76 and PILS = 0.55) for all wildfires sampled. The PILS water-soluble  
67 Abs 405 was corrected for the non-water-soluble fraction of the aerosol using the calculated  
68 UHSAS (Ultra-High-Sensitivity Aerosol Spectrometer) aerosol mass. The corrected PILS water-  
69 soluble Abs 405 showed good closure with the PAS total Abs 405 BrC with a factor of ~1.5 to 2  
70 difference. This difference was explained by particle vs. bulk solution absorption measured by  
71 the PAS vs. PILS, respectively, and confirmed by Mie Theory calculations. During WE-CAN,  
72 ~45% (ranging from 31% to 65%) of the BrC absorption was observed to be due to water-soluble  
73 species. The ratio of BrC absorption to WSOC or  $\Delta$ CO showed no clear dependence on fire  
74 dynamics or the time since emission over 9 h.

75  
76  
77  
78  
79  
80  
81  
82  
83  
84  
85  
86  
87  
88  
89  
90  
91  
92



## 93 1. Introduction

94 Organic compounds can comprise a large fraction of PM (particulate matter) mass  
95 [Kanakidou *et al.*, 2005; Zhang *et al.*, 2007]. Organic carbon can be directly emitted or formed  
96 in the atmosphere from a variety of sources. This leads to organic aerosol particles composed of  
97 a number of compounds that range from insoluble to highly water-soluble and that can scatter or  
98 absorb light [Jacobson *et al.*, 2000; Saxena and Hildemann, 1996, and references therein].  
99 The portion of organic carbon that is light-absorbing has been referred to as brown  
100 carbon (BrC) due to its yellow or brown color when concentrated, and it is likely to be a  
101 significant contributor to the visible light-absorption budget [Andreae and Gelencsér, 2006].  
102 Recent modeling studies have predicted a non-negligible effect on the Earth's radiation balance  
103 from BrC [Feng *et al.*, 2013; Zhang *et al.*, 2017; Zhang *et al.*, 2020]. Global measurements have  
104 shown that BrC can contribute up to 48% of the overall warming effect by absorbing  
105 carbonaceous aerosols [Zeng *et al.*, 2020]. BrC may also suppress photolysis rates of some  
106 chemical reactions, including decreasing surface ozone concentrations in certain locations, due to  
107 its ability to absorb at ultraviolet wavelengths [Jo *et al.*, 2016]. Some portion of BrC is likely  
108 composed of toxins, such as nitro- and oxy-aromatic species, suggesting BrC could also have  
109 health impacts [Desyaterik *et al.*, 2013; Verma *et al.*, 2015; Zhang *et al.*, 2013]. BrC itself is  
110 thought to have both primary and secondary sources. Particles from biomass burning or  
111 incomplete combustion of fossil fuels generally contain significant amounts of BrC (e.g.,  
112 [Chakrabarty *et al.*, 2010; Hoffer *et al.*, 2006; Kirchstetter *et al.*, 2004; Kirchstetter and  
113 Thatcher, 2012; Lack *et al.*, 2012; Lukács *et al.*, 2007]). Laboratory studies have observed  
114 production of BrC from a number of formation processes. This has included heterogenous  
115 reactions of isoprene on acidic aerosol particles, a variety of aqueous-phase reactions, and  
116 reactions of organic compounds in acidic solutions (e.g., [Hoffer *et al.*, 2006; Limbeck *et al.*,  
117 2013; Sareen *et al.*, 2010; Updyke *et al.*, 2012]). However, there is still limited information on  
118 the contribution of BrC to total light absorption and the sources of BrC as there are few ambient  
119 measurements.

120 Total absorption measurements (black carbon (BC) + BrC) at multiple wavelengths can  
121 be used to determine BrC absorption due to the strong wavelength dependence of BrC. This  
122 requires the assumptions that: (1) the absorption Ångström exponent (AAE) for BC is known, (2)  
123 AAE is constant with wavelength, and (3) BrC does not absorb at longer wavelengths. The AAE  
124 for BC is well constrained at 1 in the visible and near-infrared wavelengths [Moosmüller *et al.*,  
125 2009]. The BrC absorption at other wavelengths is then found by difference from the  
126 extrapolated BC AAE [Lack and Langridge, 2013; Mohr *et al.*, 2013]. This approach can be  
127 applied to any technique that measures absorption at multiple wavelengths, including  
128 photoacoustic spectroscopy (PAS).

129 BrC can also be quantified by isolating the BrC chromophores by extraction of particles  
130 in solvents, such as water or methanol, in order to separate them from the insoluble BC and then  
131 measuring the light absorption of the soluble organic chromophores [Hecobian *et al.*, 2010].  
132 This is the only direct method to separate and quantify BrC as the light absorption from liquid  
133 extracts does not suffer from interferences by BC as they can be isolated by dissolution. A  
134 spectrophotometer with an UV/Vis (ultraviolet/visible) light source can provide high spectral  
135 resolution over a wide wavelength range from 200 to 800 nm. In addition, when coupled with a  
136 long-path liquid waveguide capillary absorption cell (LWCC), it also provides a highly sensitive  
137 measurement. This technique can be used off-line with filters or on-line with an aerosol



138 collection device such as Particle-into-Liquid Sampler (PILS) (e.g., [Hecobian *et al.*, 2010; Liu  
139 *et al.*, 2013, 2014, 2015; Zhang *et al.*, 2011, 2013].

140 Here we report BrC absorption data from a PAS and PILS-LWCC-TOC system to  
141 compare total vs. water-soluble BrC absorption in wildfire smoke. Data are from smoke plume  
142 penetrations during the Western Wildfire Experiment for Cloud Chemistry, Aerosol Absorption  
143 and Nitrogen (WE-CAN), an aircraft-based study focused on investigating the chemistry and  
144 transformation of emissions from wildfires in the western U.S. We examine the relationship  
145 between the BrC absorption and species known to be from biomass burning. We discuss how  
146 parameters such as aging and fire dynamics might influence BrC absorption from wildfires.

147

## 148 **2. Methods**

### 149 **2.1. The Airborne Mission**

150 The WE-CAN Campaign was a multi-investigator study conducted aboard the National  
151 Science Foundation/National Center for Atmospheric Research (NSF/NCAR) C-130 aircraft.  
152 The C-130 was operated out of Boise, ID from Jul. 20 to Aug. 31, 2018. A suite of instruments  
153 was deployed for measurements of aerosol and trace gas composition. A total of 16 research  
154 flights sampled wildfire smoke over the western U.S. to characterize emissions, mixing,  
155 chemical transformations, and transport. Figure 1 presents a map of the flight transects and  
156 locations of the wildfires sampled. (We exclude Flight RF14, which was conducted off the coast  
157 of CA to sample a stratus deck impacted by smoke, and Flight RF16, which consisted of an  
158 intercomparison performed near Boise between WE-CAN and BB-FLUX (Biomass Burning  
159 Flux Measurements of Trace Gases and Aerosols) common measurements.) More information  
160 on each wildfire including the type of fuel consumed is available in the WE-CAN Field Catalog  
161 ([catalog.eol.ucar.edu/we-can](http://catalog.eol.ucar.edu/we-can)). WE-CAN sampled both fresh and aged (for Flights RF05 and  
162 RF08 along with parts of Flights RF07 and RF13) emissions from smoke for wildfires burning in  
163 CA, OR, WA, ID, MT, UT, and NV. The general sampling strategy was to circle the wildfire at  
164 the source and then follow the smoke downwind using a multiple transect search and rescue  
165 pattern to examine smoke evolution. Typically, wildfire smoke plumes were sampled in the free  
166 troposphere between 3-5 km during early afternoon to evening periods (20:00 to 02:00 UTC or  
167 14:00 to 20:00 LT). Flight RF08 and part of Flight RF07 were exceptions as the aircraft sampled  
168 the boundary layer (below 2 km) over the Central Valley of CA.

169

### 170 **2.2. Particle Collection**

171 During WE-CAN, we deployed two Particle-into-Liquid Sampler (PILS) systems. A  
172 PILS is an aerosol collection device that continuously collects ambient particles into purified  
173 water [Orsini *et al.*, 2003]. After particles are grown inside the body of the PILS by water  
174 condensation in a supersaturated water vapor environment, formed through mixing the ambient  
175 air sample with saturated air (100% relative humidity) at higher temperature, the particles are  
176 collected by an impactor. The impactor plate is continually washed off by a flow of liquid  
177 passed over the impactor, providing a liquid sample containing dissolved aerosol particles which  
178 can be analyzed by various methods. Each PILS system sampled from a Submicron Aerosol  
179 Inlet (SMAI) [Craig *et al.*, 2013a, 2013b, 2014; Moharreri *et al.*, 2014] mounted to the belly of  
180 the NSF/NCAR C-130. The size-cut for each PILS was provided by a nonrotating MOUDI  
181 impactor stage with a 50% transmission efficiency of 1  $\mu\text{m}$  aerodynamic diameter (i.e.,  $\text{PM}_{10}$ ) at 1  
182 atmosphere ambient pressure [Marple *et al.*, 1991]. The flowrate of 15 LPM was sampled by

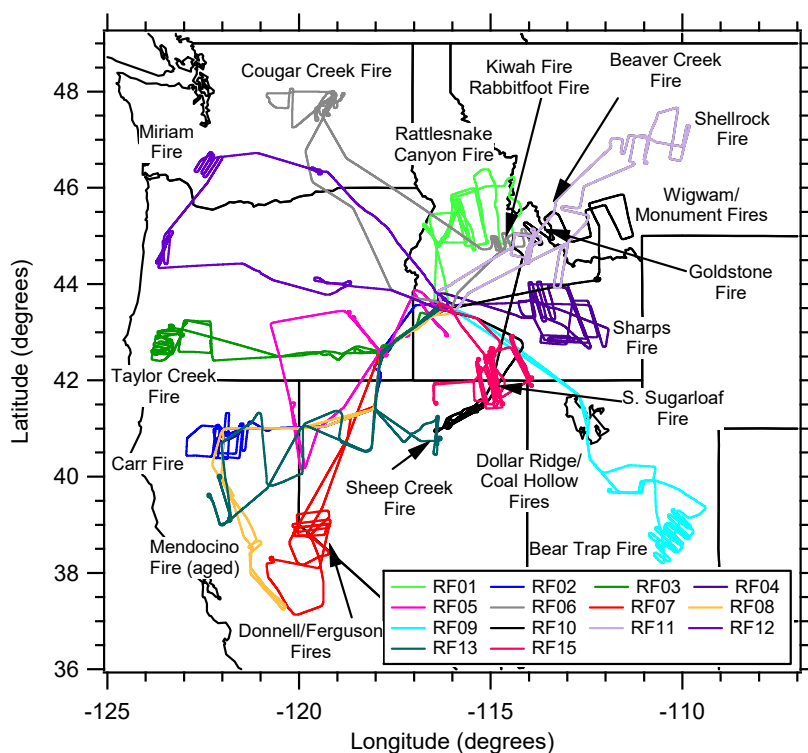


Figure 1. Map showing the flight paths and locations of the wildfires sampled during WE-CAN used in this analysis.

183  
184  
185

186 each PILS through the inlet and MOUDI stage. An activated carbon parallel plate denuder  
187 [Eatough *et al.*, 1993] was situated upstream of both PILS to remove organic gases. In addition,  
188 for PILS2 two honeycomb denuders coated with sodium carbonate and phosphorous acid were  
189 used to remove inorganic acidic and basic gases in order to limit possible positive artifacts from  
190 dissolving in the PILS collection liquid. PILS 1 was connected to a LWCC (liquid waveguide  
191 capillary cell) and TOC (Total Organic Carbon) Analyzer for near real-time measurement of  
192 water-soluble BrC (Brown Carbon) absorption and WSOC (water-soluble organic carbon),  
193 respectively. PILS2 was coupled to a Bretchel fraction collector system [Sorooshian *et al.*,  
194 2006] to provide liquid samples for additional off-line analysis.

195 For PILS 1, a valve upstream of the PILS was manually closed periodically for 10 min  
196 forcing the airflow through a Teflon filter allowing for a measurement of the background in near  
197 real-time. The liquid sample obtained from PILS1 was then pushed through a 0.2  $\mu\text{m}$  PTFE  
198 liquid filter at a flowrate of 1.2 mL/min by a set of syringe pumps with 1 mL syringes to ensure  
199 any insoluble particles were removed before passing through the LWCC and TOC Analyzer.

200 A LWCC with a 2.5 m path-length (World Precision Instruments, Sarasota, FL) was  
201 employed. An absorption spectrometer (FLAME-T-UV-VIS, Ocean Optics, Largo, FL) and dual  
202 deuterium and tungsten halogen light source (DH-mini, Ocean Optics, Largo, FL) were coupled



203 to the LWCC via fiber optic cables. The Oceanview Spectroscopy Software was used to record  
204 absorption spectra over a range from 200 to 800 nm. In this paper we present the absorption  
205 determined at 365 and 405 nm. This wavelength dependent absorption was calculated following  
206 the method outlined in *Hecobian et al.* [2010]. A 16 s integrated measurement of water-soluble  
207 absorption with a limit of detection (LOD) of  $0.1 \text{ Mm}^{-1}$  was obtained.

208 A Sievers Model M9 Portable TOC Analyzer (Suez Waters Analytical Instruments,  
209 Boulder, CO) was used for the WSOC measurement. This analyzer converts organic carbon in  
210 the liquid sample to carbon dioxide using chemical oxidation with ammonium persulfate and  
211 ultraviolet light. The carbon dioxide formed is then measured by conductivity. The amount of  
212 OC present in the sample is proportional to the increase in conductivity observed. The analyzer  
213 was run in turbo mode providing a 4 s integrated measurement of WSOC with a LOD of  $0.1 \mu\text{g}$   
214  $\text{C}/\text{m}^3$ .

215 For PILS2, a valve upstream of the PILS was manually closed periodically for 10 min  
216 forcing the airflow through a hepa filter allowing for measurement of the background in near  
217 real-time. The liquid sample obtained from PILS2 was pushed into the fraction collector vials at  
218 a flowrate of  $0.65 \text{ mL}/\text{min}$  by a peristaltic pump for collection of  $\sim 1.2 \text{ mL}$  of liquid sample per  
219 vial. Each fraction collector carousel holds 72  $1.5 \text{ mL}$  polypropylene vials (Microsolv  
220 Technology Corporation, Leland, NC). Vials were fitted with pre-slit caps and used as supplied.  
221 The fraction collector program was set to allow continuous collection of 2 min integrated  
222 samples and was manually started after take-off. Carousels were pre-loaded before flight and  
223 then manually switched out as they were filled. The vials were unloaded from the carousels at  
224 the end of each flight, recapped with solid caps (Microsolv Technology Corporation), packed in  
225 coolers with ice packs, and shipped back to Colorado State University to be stored in a  $2 \text{ }^\circ\text{C}$  cold  
226 room until analysis began following completion of the study.

227

### 228 **2.3. Off-line Analysis**

229 Each fraction collector vial was brought to room temperature and then analyzed for  
230 levoglucosan as well as a suite of anions/organic acids and cations. For each analysis,  $300 \mu\text{L}$   
231 aliquots were transferred to polypropylene vials. Only levoglucosan, water-soluble potassium,  
232 and ammonium are discussed here and their analytical methods are explained below.

233 The levoglucosan analysis was performed on a Dionex DX-500 series ion chromatograph  
234 with pulsed amperometric detection via an ED-50/ED-50A electrochemical cell. This cell  
235 includes two electrodes: a “standard” gold working electrode and pH-Ag/AgCl (silver/silver  
236 chloride) reference electrode. A sodium hydroxide gradient and a Dionex CarboPac PA-1  
237 column ( $4 \times 250 \text{ mm}$ ) were employed for the separation. The complete run time was 59 min  
238 with an injection volume of  $100 \mu\text{L}$ . More details on the method can be found in *Sullivan et al.*  
239 [2011a,b, 2014, 2019]. Only levoglucosan could be detected in the WE-CAN samples (other less  
240 abundant anhydrosugars were too low to detect in the PILS samples) and did not require  
241 background correction. The LOD for levoglucosan based on a sample collection time of 2 min  
242 and air flowrate of 15 LPM was determined to be less than approximately  $0.10 \text{ ng}/\text{m}^3$ .

243 A Dionex ICS-3000 ion chromatograph was used to measure water-soluble potassium  
244 and ammonium. An eluent generator provided a concentration of 20 mM methanesulfonic acid  
245 at a flowrate of  $0.5 \text{ mL}/\text{min}$  to perform the separation on a Dionex IonPac CS12A analytical  
246 column ( $3 \times 150 \text{ mm}$ ). The complete run time was 17 min with an injection volume of  $190 \mu\text{L}$ .  
247 A blank correction was necessary for both of these species unlike levoglucosan. Therefore, their



248 concentrations were corrected by using the average of all background samples collected during a  
249 specific flight. For water-soluble potassium and ammonium, the LOD was  $1 \text{ ng/m}^3$ .

250

#### 251 **2.4. Photoacoustic Aerosol Absorption Spectrometer**

252 A custom-built PAS was used to measure total aerosol absorption at 405 and 660 nm  
253 [Foster *et al.*, 2019] every 1 s during WE-CAN. The PAS measures aerosol light absorption at  
254 near-ambient conditions by heating particles using a controlled light source and detecting the  
255 resulting soundwave. It can be subject to interference by gaseous absorbers and is sensitive to  
256 variations in relative humidity, temperature, and pressure [Arnott *et al.*, 1999; Langridge *et al.*,  
257 2013]. The PAS sampled from a Solid Diffuser Inlet (SDI) mounted on the front right side of the  
258 NSF/NCAR C-130. Aerosol passed through a cyclone impactor before entering the PAS to  
259 remove particles with aerodynamic diameters  $> 1 \mu\text{m}$ . The flowrate for the PAS was 4 LPM.  
260 Upstream of the PAS was a denuder to remove  $\text{NO}_x$  (nitrogen oxides) from the sample air as  
261 well as a Perma Pure dryer to dry the aerosol to below 30% relative humidity. A filter was  
262 periodically switched in-line before the PAS to remove particles and allow for a near real-time  
263 measurement of the baseline stability. Additionally, the PAS switched between sampling with  
264 and without a thermal denuder system in-line. Only the data from sampling without the thermal  
265 denuder is presented here. The PAS BrC absorption at 405 nm (PAS total Abs 405 BrC) was  
266 calculated using equation 9 from Pokhrel *et al.* [2017]. This approach assumes the absorption  
267 determined by the PAS at 660 nm was equivalent to BC absorption and the BC aerosol AAE was  
268 1.

269

#### 270 **2.5. Ultra-High-Sensitivity Aerosol Spectrometer**

271 One second particle number concentrations were measured using a rack-mounted  
272 UHSAS (Ultra-High-Sensitivity Aerosol Spectrometer). The rack-mounted UHSAS switched  
273 between sampling from the SDI inlet and a CVI (counter-flow virtual impactor) when sampling  
274 out of and in-cloud, respectively. We only present data for sampling out of clouds. The rack-  
275 mounted UHSAS was operated so that the flow could be manually lowered by the in-flight  
276 operator when the NSF/NCAR C-130 flew through smoke plumes to allow the UHSAS to stay  
277 within its optimum concentration measurement range. The particle size bins for the UHSAS  
278 were calibrated using ammonium sulfate rather than traditional PSL (polystyrene latex) spheres.  
279 Particle mass concentrations for  $\text{PM}_{10}$  were calculated by applying these size bins and then  
280 multiplying by  $1.4 \text{ g/cm}^3$  to account for particle density.

281

#### 282 **2.6. Other Measurements**

283 In the following analysis, we focus on characterizing the BrC absorption in smoke from  
284 wildfires in the western U.S. sampled during WE-CAN. Other airborne measurements used in  
285 this analysis include meteorological data and coordinates provided by the Research Aviation  
286 Facility (RAF) as part of the C-130 instrumentation package  
287 (<https://data.eol.ucar.edu/project/WE-CAN>) and one Hz carbon monoxide (CO) determined by a  
288 vacuum UV (ultraviolet) resonance fluorescence method [Gerbig *et al.*, 1999]. All data  
289 presented in our analysis are reported at 1 atm and 273 K. Data from all species have been  
290 averaged to match the 2 min collection time of the PILS-fraction collector system.

291

#### 292 **2.7. Mie Calculation**



293 Mie calculations were performed by putting the complex refractive index ( $m = n + ik$ ) into  
294 Mie code to obtain the absorption efficiency ( $Q$ ) and then further calculate the absorption  
295 coefficient using Eq. 1 [Liu *et al.*, 2013]. The real part of the refractive index ( $n$ ) was set to be  
296 1.55 and the imaginary part was calculated using Eq. 2 [Liu *et al.*, 2013].  
297

$$298 \quad \beta(\lambda, D_p) = \frac{3}{2} \cdot \frac{Q \cdot WSOC}{D_p \cdot \rho} \quad (Eq. 1)$$

299

$$300 \quad k = \frac{\rho \lambda \cdot H_2O\_ \beta(\lambda)}{4\pi \cdot WSOC} \quad (Eq. 2)$$

301

302 In Eq. 1 and 2,  $\lambda$  is the wavelength,  $D_p$  is the diameter of the particle,  $\beta$  is the absorption  
303 coefficient (referred to as the Mie calculated water-soluble absorption hereinafter),  $Q$  is the  
304 absorption efficiency,  $WSOC$  is the water-soluble organic carbon mass concentration measured  
305 by the PILS, and  $H_2O\_ \beta(\lambda)$  is the water-soluble light absorption coefficient measured by the  
306 PILS. The particle density ( $\rho$ ) was assumed to be  $1.4 \text{ g/cm}^3$ . The plume averaged particle size  
307 distribution (measured by the UHSAS) was used in the calculation. The Mie calculated water-  
308 soluble absorption was determined for each size bin in order to obtain the most accurate results.  
309 Mie calculated total absorption was further calculated by multiplying the Mie calculated water-  
310 soluble absorption by (UHSAS mass)/(WSOC\*1.6), where the factor of 1.6 was to convert  
311 WSOC to WSOM (water-soluble organic matter) [Duarte *et al.*, 2019; Yttri *et al.*, 2007].  
312

312

### 313 **3. Results and Discussion**

#### 314 **3.1. Overview**

315 Most previous studies employing a LWCC to determine water-soluble absorption,  
316 examine the absorption at 365 nm (e.g., [Hecobian *et al.*, 2010; Zhang *et al.*, 2011, 2013]. But  
317 here in order to explore the relationship between the water-soluble and total absorption  
318 determined by the PILS and PAS, respectively, we focus on the absorption at 405 nm determined  
319 by the LWCC. Using as examples Flight RF02, which sampled the Carr Fire smoke plume, and  
320 Flight RF11, which sampled the Goldstone, Rabbit Foot, Beaver Creek, and Shellrock Fire  
321 smoke plumes, Figures 2a and b show the relationship of the PILS water-soluble Abs 405 vs.  
322 Abs 365. Absorption values at these two wavelengths are correlated ( $R^2$  values from 0.70 to  
323 1.00 based on all individual WE-CAN Flights), but the absorption measured at 405 nm was  
324 about half of that observed at 365 nm (slope average 0.45 and range from 0.39 to 0.52 across all  
325 individual WE-CAN flights).

326 Figure 3 shows example time series for WSOC, PILS water-soluble Abs 405, and PAS  
327 total Abs 405 BrC from the same two flights as above. It was observed that all three parameters  
328 tracked each other in and out of the smoke plumes. During WE-CAN, the average value  $\pm$   
329 standard deviation for WSOC, PILS water-soluble Abs 405, and PAS total Abs 405 BrC were  
330  $13.35 \pm 16.80 \text{ } \mu\text{g C/m}^3$ ,  $6.06 \pm 6.88 \text{ Mm}^{-1}$ , and  $22.02 \pm 49.16 \text{ Mm}^{-1}$ , respectively. The water-  
331 soluble absorption determined by the PILS was lower than the total absorption determined by the  
332 PAS. This pattern was consistently observed for all the wildfires sampled throughout WE-CAN.  
333

333

334

335



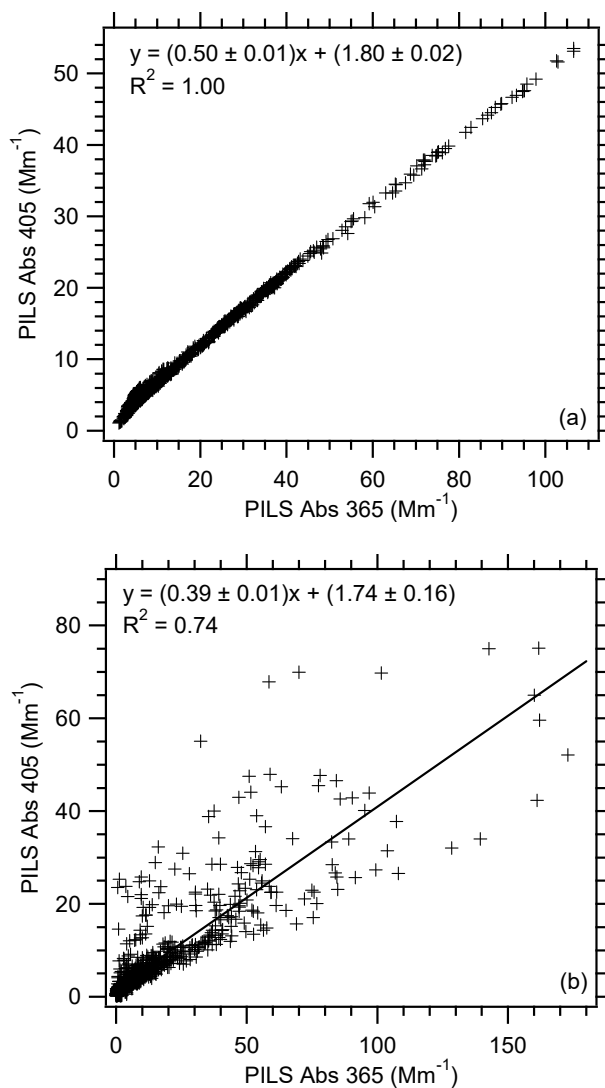


Figure 2. Correlation of PILS water-soluble Abs 405 vs. PILS water-soluble Abs 365 for WE-CAN (a) Flight RF02 and (b) Flight RF11. Uncertainties with the least square regressions are one standard deviation.

336  
337  
338  
339  
340  
341  
342  
343

### 3.2. Relationship between Total and Water-Soluble BrC Absorption

To further explore the relationship between total and water-soluble BrC absorption, we examine the relationship between PAS total Abs 405 BrC and UHSAS mass for Flights RF02 and RF11. There is a strong correlation between PAS total Abs 405 BrC and UHSAS mass (Figure 4). Therefore, the PILS water-soluble Abs 405 can be corrected for the non-water-

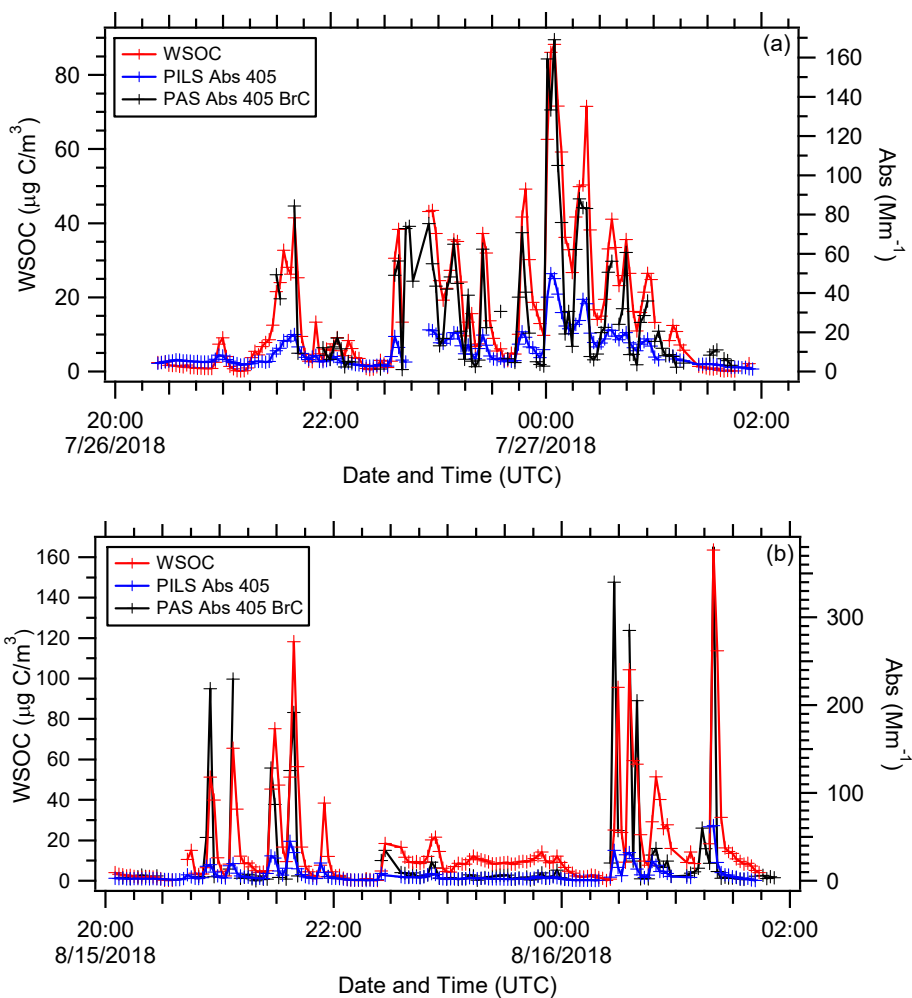


Figure 3. Time series of WSOC, PILS water-soluble Abs 405, and PAS total Abs 405 BrC for WE-CAN (a) Flight RF02 and (b) Flight RF11.

344

345

346

347 soluble fraction of the aerosol using the UHSAS mass. This was achieved by multiplying the  
348 PILS water-soluble Abs 405 by  $1/((\text{WSOC} \cdot 1.6)/(\text{UHSAS mass}))$ . This approach assumes the  
349 water-soluble and non-water-soluble components of OC are the same.

350 Correcting the PILS water-soluble Abs 405 by the UHSAS mass showed good closure  
351 with the PAS total Abs 405 BrC, but with a factor of  $\sim 1.5$  to 2 difference between the PILS  
352 water-soluble Abs 405 corrected and PAS total Abs 405 BrC (Figures 4c and d). This is also  
353 similar to results obtained from the sampling of wildfire smoke during the FIREX (Fire Influence  
354 on Regional and Global Environments Experiment) Campaign, where there was a ratio of 3.2  
355 between PAS Abs 405 BrC and water-soluble Abs 405 determined from off-line LWCC analysis

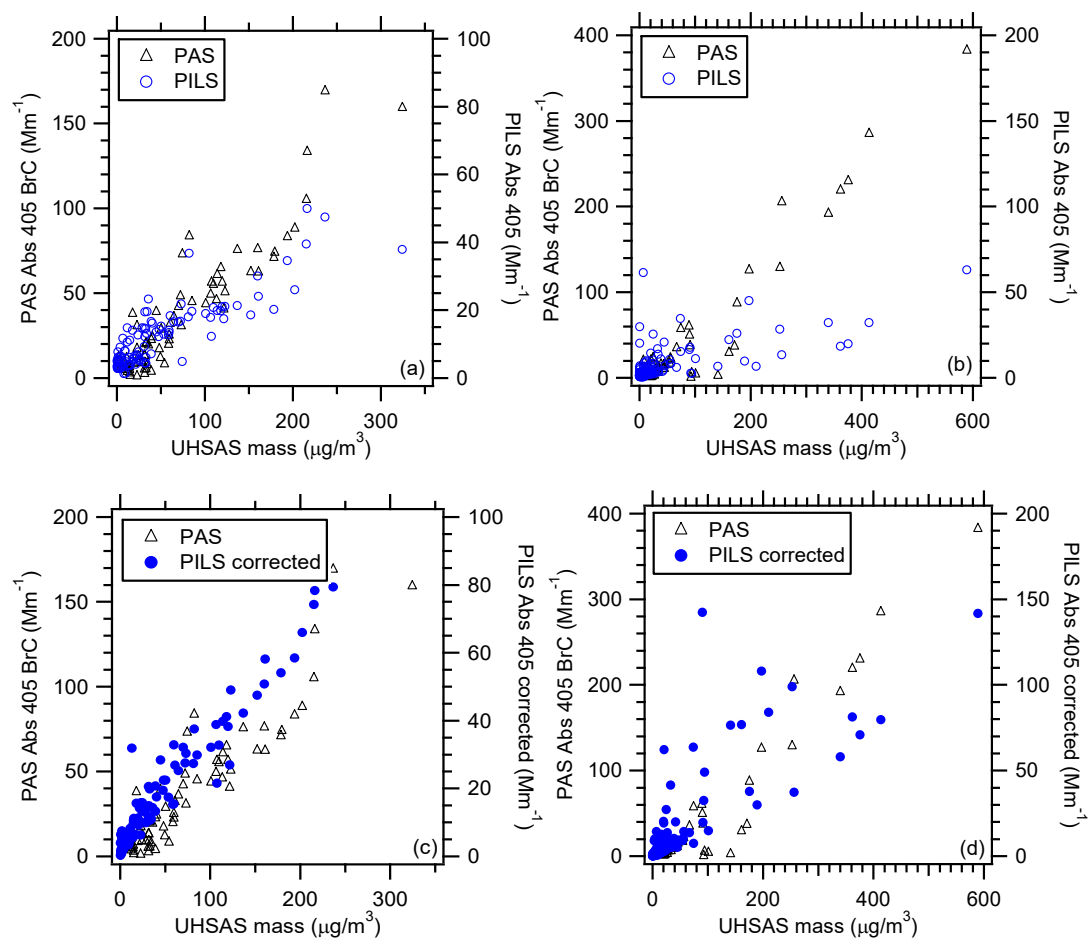


Figure 4. Correlation of PAS total Abs 405 BrC and PILS water-soluble Abs 405 vs. UHSAS mass for WE-CAN (a) Flight RF02 and (b) Flight RF11. Correlation of PAS total Abs 405 BrC and PILS water-soluble Abs 405 corrected for the non-water-soluble fraction of the aerosol using the UHSAS mass for WE-CAN (c) Flight RF02 and (d) Flight RF11.

356  
357  
358  
359  
360  
361  
362  
363  
364  
365  
366  
367

of filter samples [Zeng *et al.*, 2020]. This factor difference in both the WE-CAN and FIREX data is likely due to the differences in particle vs. bulk solution absorption measured by the PAS vs. LWCC (using PILS or filter samples), respectively, and can be explained by Mie Theory.

We used Mie Theory to calculate the water-soluble and total particle Abs 405 (see section 2.7) through each plume transect for RF02 and RF11. As shown in Figures 5a and b, we found a slope of 1.7 to 1.8 for Mie calculated water-soluble Abs 405 to PILS Abs 405 and 3 to 4 for Mie calculated total Abs 405 to PILS Abs 405. This is similar to results presented in Liu *et al.* [2013] and based on off-line LWCC analysis of filter samples collected at 3 sites in Georgia. In that work, a ratio of 2 for Mie calculated water-soluble Abs 365 to measured water-soluble Abs 365



368 and a ratio of 3.6 for Mie calculated total Abs 365 to measured water-soluble Abs 365 were  
369 observed. In *Zeng et al.* [2022], Mie Theory was used to calculate the factor to convert solution  
370 to particle light absorption (i.e., ratio of Mie calculated to measured water-soluble absorption) as  
371 a function of wavelength for the FIREX data. At 405 nm a factor of  $\sim 1.7$  was determined,  
372 similar to what was determined from the WE-CAN data.

373 As a further check on the calculations performed here, the PAS Abs 405 BrC was  
374 compared to the Mie calculated total Abs 405. Slopes ranged from 1.04 to 1.08 (Figures 5c and  
375 d). This suggested our approach for correcting the PILS water-soluble Abs 405 for the non-  
376 water-soluble fraction as well as to calculate the BrC absorption from the PAS Abs 405 data  
377 were valid.

378 Overall, during WE-CAN  $\sim 45\%$  (ranging from 31% to 65%) of the BrC absorption at  
379 Abs 405 was due to water-soluble species. This is similar to what was observed from off-line  
380 LWCC analysis of water and methanol extracts from filter samples collected during sampling of  
381 biomass burning plumes as part of the DC3 (Deep Convective Clouds and Chemistry),  
382 SEAC4RS (Studies of Emissions, Atmospheric Composition, Clouds and Climate Coupling by  
383 Regional Surveys), and FIREX aircraft campaigns [*Forrister et al.*, 2015; *Liu et al.*, 2015; *Zeng*  
384 *et al.*, 2022].

### 385 386 **3.3. BrC Absorption, CO, WSOC, and Levoglucosan**

387 Using data from all WE-CAN flights, Figure 6 shows that the PAS total Abs 405 BrC and  
388 PILS water-soluble Abs 405 are correlated with CO ( $R^2$  value for PAS = 0.76 and PILS = 0.55).  
389 This further illustrates the importance of biomass burning as a source of BrC absorption (e.g.,  
390 [*Andreae and Gelencsér*, 2006; *Chakrabarty et al.*, 2010; *Duarte et al.*, 2005; *Hecobian et al.*,  
391 2010; *Hoffer et al.*, 2006; *Lack et al.*, 2012; *Lukács et al.*, 2007]).

392 Figure 7 shows that there is a correlation between BrC absorption and WSOC ( $R^2$  value  
393 for PAS = 0.42 and PILS = 0.60). This is not surprising given that the two main sources of  
394 WSOC are typically biomass burning and secondary organic aerosol (SOA) [*Sullivan et al.*,  
395 2006]. A number of previous studies where the source of WSOC and Abs 365 was one or both  
396 of these have observed a similar correlation (e.g., [*Hecobian et al.*, 2010; *Liu et al.*, 2015; *Zhang*  
397 *et al.*, 2013]). Additionally, analysis of cloud water samples impacted by biomass burning has  
398 shown that nitrophenols and nitrocatechol are major contributors to the light absorption between  
399 300 and 400 nm [*Desyaterik et al.*, 2013].

400 BrC absorption has a similar relationship with CO and WSOC as the biomass burning  
401 marker levoglucosan [*Simoneit et al.*, 1999], but there are additional features (Figures 8a and b).  
402 There is some variability in the ratio of levoglucosan to the PAS total Abs 405 BrC and PILS  
403 water-soluble Abs 405 between wildfires, and this leads to two branches (Branch 1 and Branch  
404 2). This was also observed for levoglucosan vs. WSOC (not shown). While there is no overall  
405 correlation of levoglucosan vs. BrC absorption across all flights, there are correlations between  
406 these two species on an individual flight basis (e.g.,  $R^2$  value for Flight RF02 = 0.76 and Flight  
407 RF11 = 0.60, not shown). When data from all flights are colored by the water-soluble potassium  
408 concentration (Figures 8c and d), we observe that Branch 1, which had the highest levoglucosan  
409 concentrations, also has the highest water-soluble potassium concentrations ( $> 0.5 \mu\text{g}/\text{m}^3$ ).  
410 Levoglucosan and BrC absorption are much more highly correlated in Branch 1, than in Branch  
411 2 for both the PILS ( $R^2$  values Branch 1 = 0.76 and Branch 2 = 0.35) and PAS ( $R^2$  values Branch  
412 1 = 0.60 and Branch 2 = 0.22) BrC absorption. To further examine this, the times series of PILS  
413

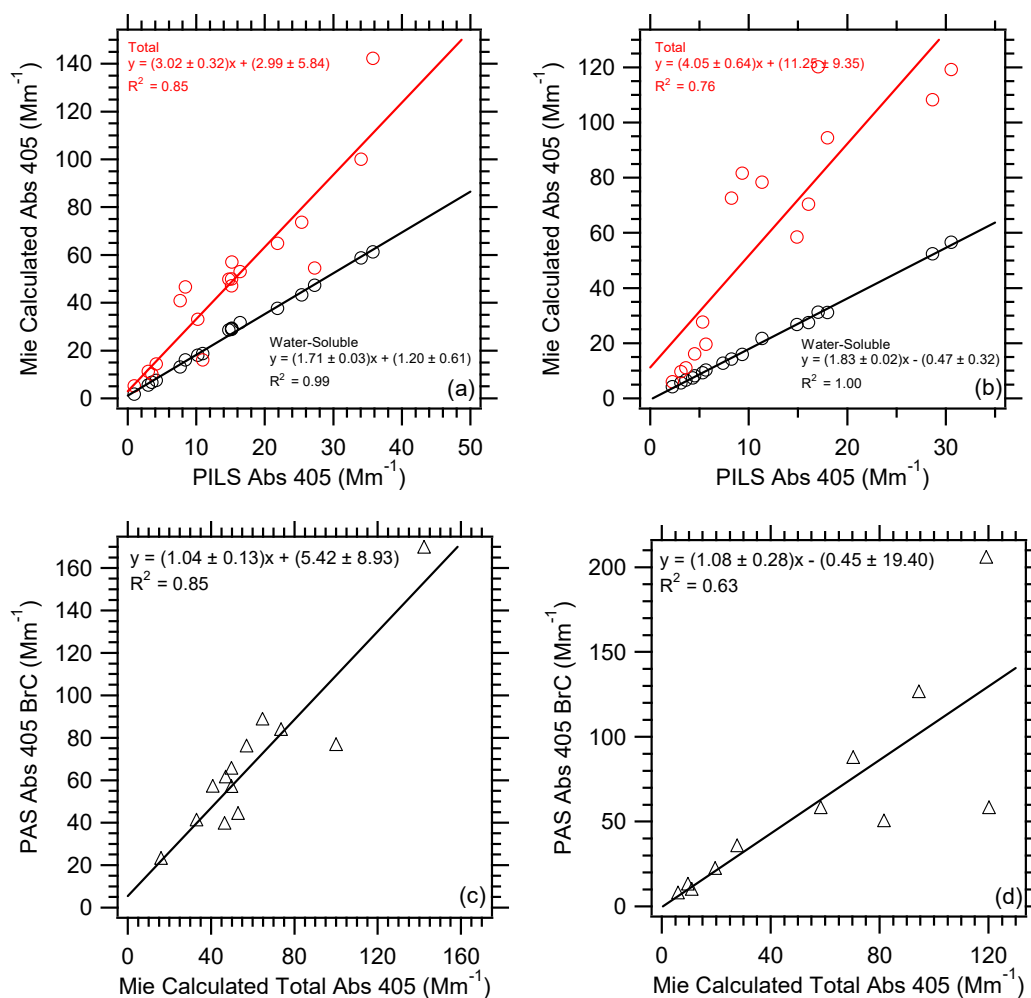


Figure 5. Correlation of Mie calculated water-soluble and total Abs 405 vs. PILS water-soluble Abs 405 for WE-CAN (a) Flight RF02 and (b) Flight RF11. Correlation of PAS total Abs 405 BrC and Mie calculated total Abs 405 for WE-CAN (c) Flight RF02 and (d) Flight RF11. Uncertainties with the least square regressions are one standard deviation.

414  
415  
416  
417  
418  
419  
420  
421  
422  
423

water-soluble Abs 405, levoglucosan, potassium, and ammonium for Flights RF02 and RF11 are shown in Figure 9. Smoke impacted samples in Flight RF02 had higher concentrations of levoglucosan and water-soluble potassium and contributed to Branch 1. The data from Flight RF11 contributed to Branch 2. In addition, elevated water-soluble potassium was observed in many of the plume intercepts during Flight RF02. But more elevated ammonium was observed for Flight RF11, which became even more prominent in smoke intercepts after 00:00 UTC, while water-soluble potassium was relatively less abundant. Water-soluble potassium is a known

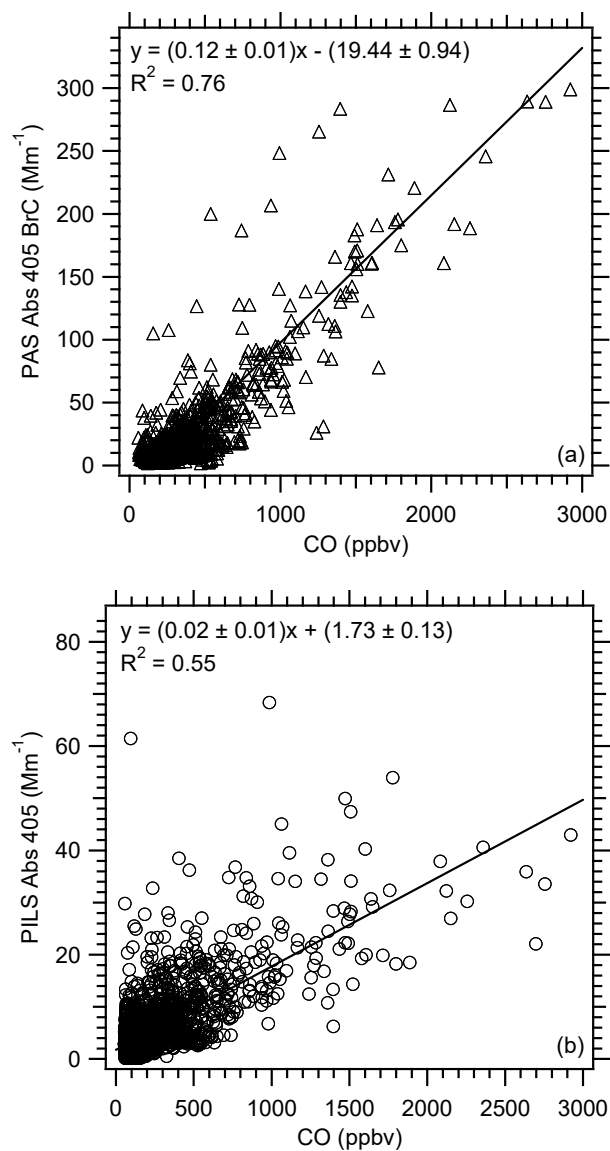


Figure 6. Correlation of (a) PAS total Abs 405 BrC and (b) PILS water-soluble Abs 405 vs. CO for all WE-CAN flights used in this analysis. Uncertainties with the least square regressions are one standard deviation.

424  
425  
426  
427  
428  
429

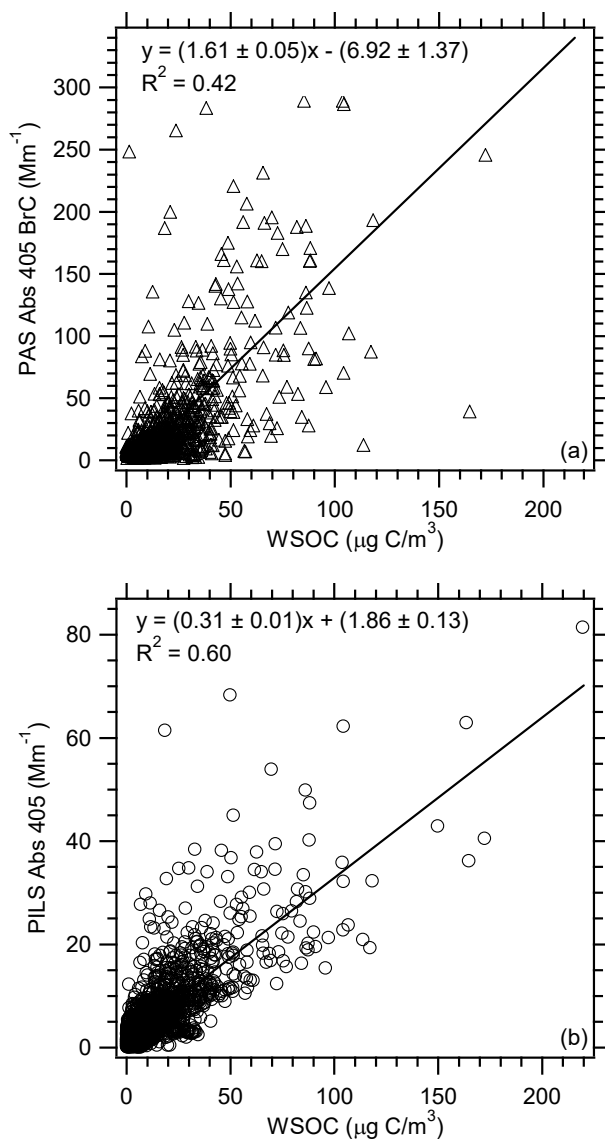


Figure 7. Correlation of (a) PAS total Abs 405 BrC and (b) PILS water-soluble Abs 405 vs. WSOC for all WE-CAN flights used in this analysis. Uncertainties with the least square regressions are one standard deviation.

430  
431  
432  
433  
434  
435

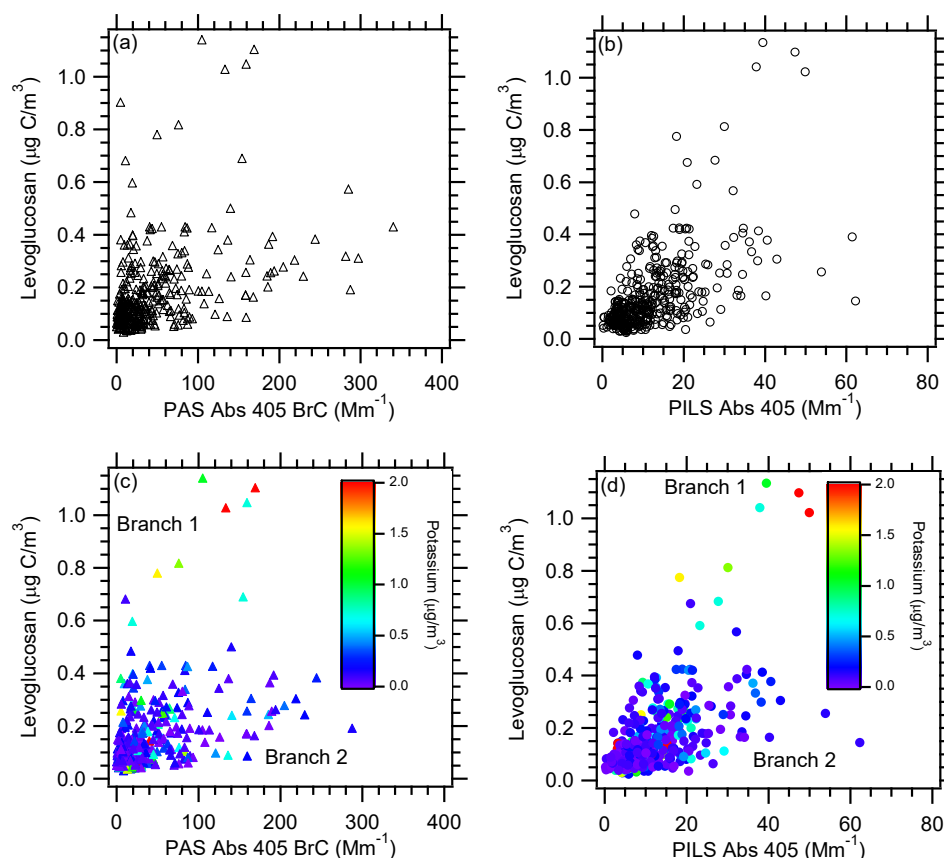


Figure 8. Correlations of levoglucosan on a carbon mass basis vs. (a) PAS total Abs 405 BrC and (b) PILS water-soluble Abs 405 for all WE-CAN flights used in this analysis. Plots (c) and (d) are the same as plots (a) and (b), but with the data colored by the PILS water-soluble potassium concentrations. Branch 1 represents data with water-soluble potassium concentrations  $> 0.5 \mu\text{g}/\text{m}^3$  and Branch 2  $< 0.5 \mu\text{g}/\text{m}^3$ . In plot (c), the equation for the fit and  $R^2$  value for Branch 1 are  $y = (0.006 \pm 0.001)x + (0.027 \pm 0.049)$ ,  $R^2 = 0.60$  and for Branch 2  $y = (0.001 \pm 0.001)x + (0.118 \pm 0.006)$ ,  $R^2 = 0.22$ , respectively. In plot (d), the equation for the fit and  $R^2$  value for Branch 1 are  $y = (0.024 \pm 0.002)x - (0.081 \pm 0.038)$ ,  $R^2 = 0.76$  and for Branch 2  $y = (0.006 \pm 0.001)x + (0.073 \pm 0.007)$ ,  $R^2 = 0.35$ , respectively. Uncertainties with the least square regressions are one standard deviation.

436  
437  
438  
439  
440  
441  
442  
443  
444

inorganic marker for biomass burning, although it is not as specific of a marker as levoglucosan as there are additional possible sources for water-soluble potassium [Schauer *et al.*, 2001] and water-soluble potassium is predominately emitted during only the flaming phase of a fire [Lee *et al.*, 2010]. These results from WE-CAN suggest there may be a relationship between levoglucosan and water-soluble potassium in wildfire emissions that has not been observed in other types of burning [Sullivan *et al.*, 2014, 2019].



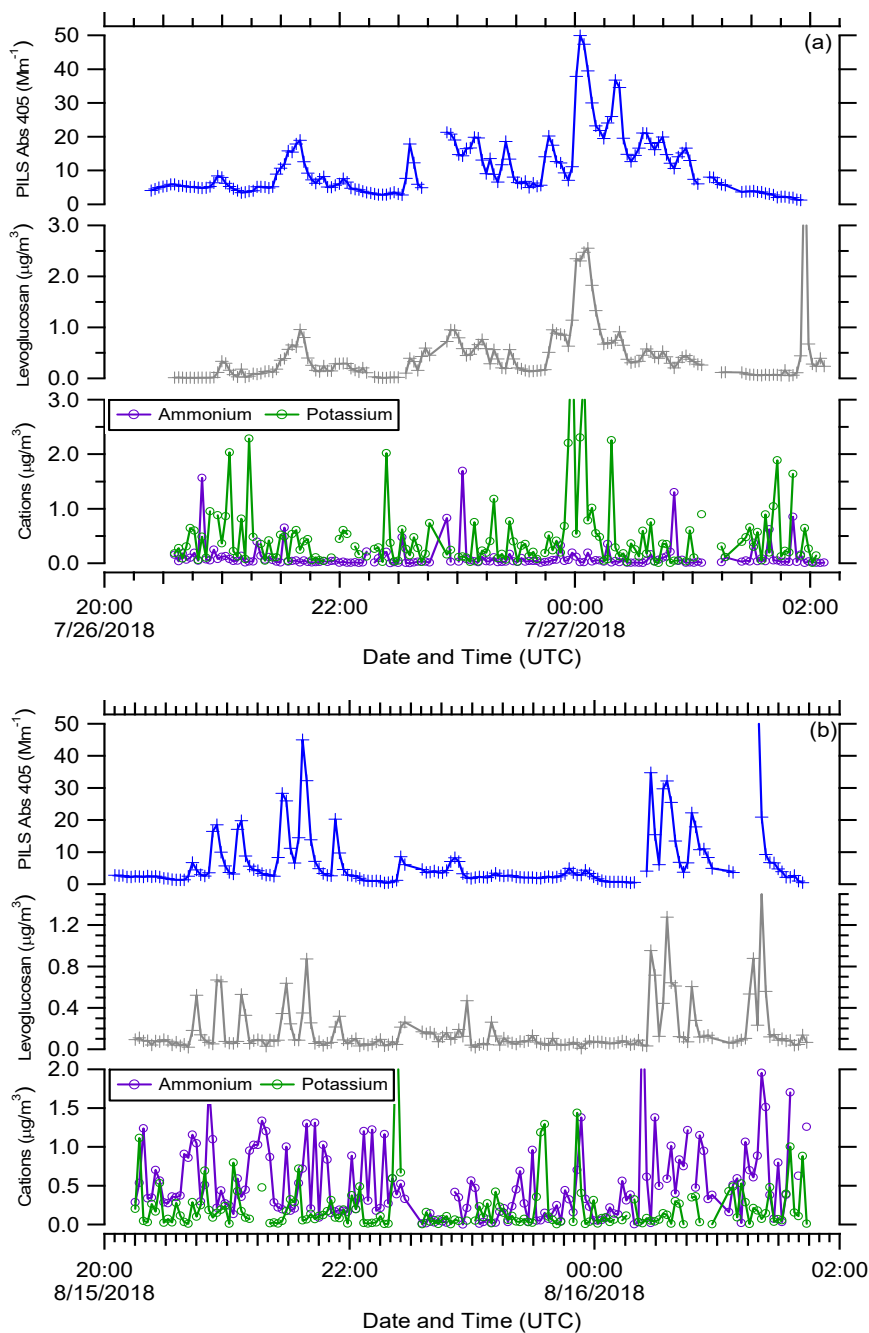


Figure 9. Time series from top to bottom of PILS water-soluble Abs 405, PILS levoglucosan, and PILS ammonium and water-soluble potassium for WE-CAN (a) Flight RF02 and (b) Flight RF11.



### 446 3.4. Evolution of BrC Absorption with Plume Age and Fire Dynamics

447 The time since emission (i.e., the smoke age) was estimated for all possible wildfire  
448 plumes as the distance the plume was sampled from the source divided by the average wind  
449 speed at that particular sampling altitude. Only PILS-fraction collector samples that directly  
450 overlapped with a CO plume penetration are considered. To account for dilution, we normalized  
451 the BrC absorption to 3 different species. We examine the ratio of BrC absorption to WSOC,  
452  $\Delta\text{CO}$  (assuming a CO background of 100 ppbv), and levoglucosan.

453 Figure 10a presents the ratio of PAS total Abs 405 BrC to WSOC and PILS water-soluble  
454 Abs 405 to WSOC, Figure 10b presents the ratio of PAS total Abs 405 BrC to  $\Delta\text{CO}$  and PILS  
455 water-soluble Abs 405 to  $\Delta\text{CO}$ , and Figure 10c presents the ratio of PAS total Abs 405 BrC to  
456 levoglucosan and PILS water-soluble Abs 405 to levoglucosan as a function of time since  
457 emission. Figures S1-S3 show these 3 ratios for each smoke plume individually. If WSOC was  
458 lost with age due to evaporation of more volatile components or SOA formation were occurring  
459 with time since emission, CO would be expected to be more stable. It appears, however, that a  
460 similar pattern, perhaps with a bit more scatter for Abs 405 to WSOC, is observed for all of these  
461 ratios. Within a particular wildfire, there is no clear evidence that the PILS water-soluble BrC  
462 absorption is affected by smoke age up to 9 h. For the PAS total BrC absorption, especially for  
463 the ratio to  $\Delta\text{CO}$ , there appears to be a possible decrease in the ratio in the first 2 h, suggesting a  
464 need to further explore changes in total BrC absorption near the source region.

465 A number of laboratory studies suggest the initial stages of photochemical aging  
466 increases light absorption (i.e., photoenhancement). This is then followed by a decrease in light  
467 absorption (i.e., photobleaching) [Hems and Abbatt, 2018; Saleh *et al.*, 2013; Sumlin *et al.*, 2017;  
468 Zhao *et al.*, 2015; Zhong and Jang, 2014]. However, it is challenging to directly compare this  
469 laboratory data to the ambient data collected during WE-CAN. But analysis of laboratory and  
470 ambient biomass burning samples by Wong *et al.* [2019], found low molecular weight (< 400  
471 Da) BrC undergoes rapid photobleaching on timescales of a few h, but high molecular weight (>  
472 400 Da) BrC was stable for up to a few days. This suggest that the BrC sampled during WE-  
473 CAN could be composed mainly of high molecular weight species.

474 In addition, to investigate these ratios as a function of time since emission, the WE-CAN  
475 data had to be integrated across a smoke plume in order to incorporate the PILS-fraction  
476 collector measurements. Of course, a smoke plume itself was dynamic with concentrations  
477 being highest in the middle of the plume and more dilute on the edges. It is possible the  
478 averaging could contribute to the observed pattern of BrC absorption not changing with age.  
479 Forrister *et al.* [2015], who used plume transect averages of SEAC4RS data, reported a decrease  
480 in the total Abs 365/ $\Delta\text{CO}$  from  $\sim 0.13$  to  $0.07 \text{ Mm}^{-1}/\text{ppbv}$  in 5 h for smoke from the Rim Fire.  
481 Observations of smoke during FIREX, by contrast, indicated no clear trend with plume age  
482 [Zeng *et al.*, 2022] in a dataset where the majority of plume ages were less than 10 h. These  
483 varying results also suggest that other factors that contribute to changes in BrC absorption over  
484 time may still need to be explored.

485 In order to investigate the possible influence of fire dynamics on BrC absorption, the  
486 modified combustion efficiency (MCE) was calculated as the change in carbon dioxide divided  
487 by the sum of the change in carbon monoxide and carbon dioxide ( $\Delta\text{CO}_2/(\Delta\text{CO} + \Delta\text{CO}_2)$ ) on a  
488 molar basis [Ward and Radke, 1993]. A higher MCE value indicates a more intense or extended  
489 flaming phase as opposed to a smoldering phase. Within a particular wildfire there appeared to  
490 be no clear dependence of the ratio of BrC absorption to WSOC,  $\Delta\text{CO}$ , or levoglucosan on MCE

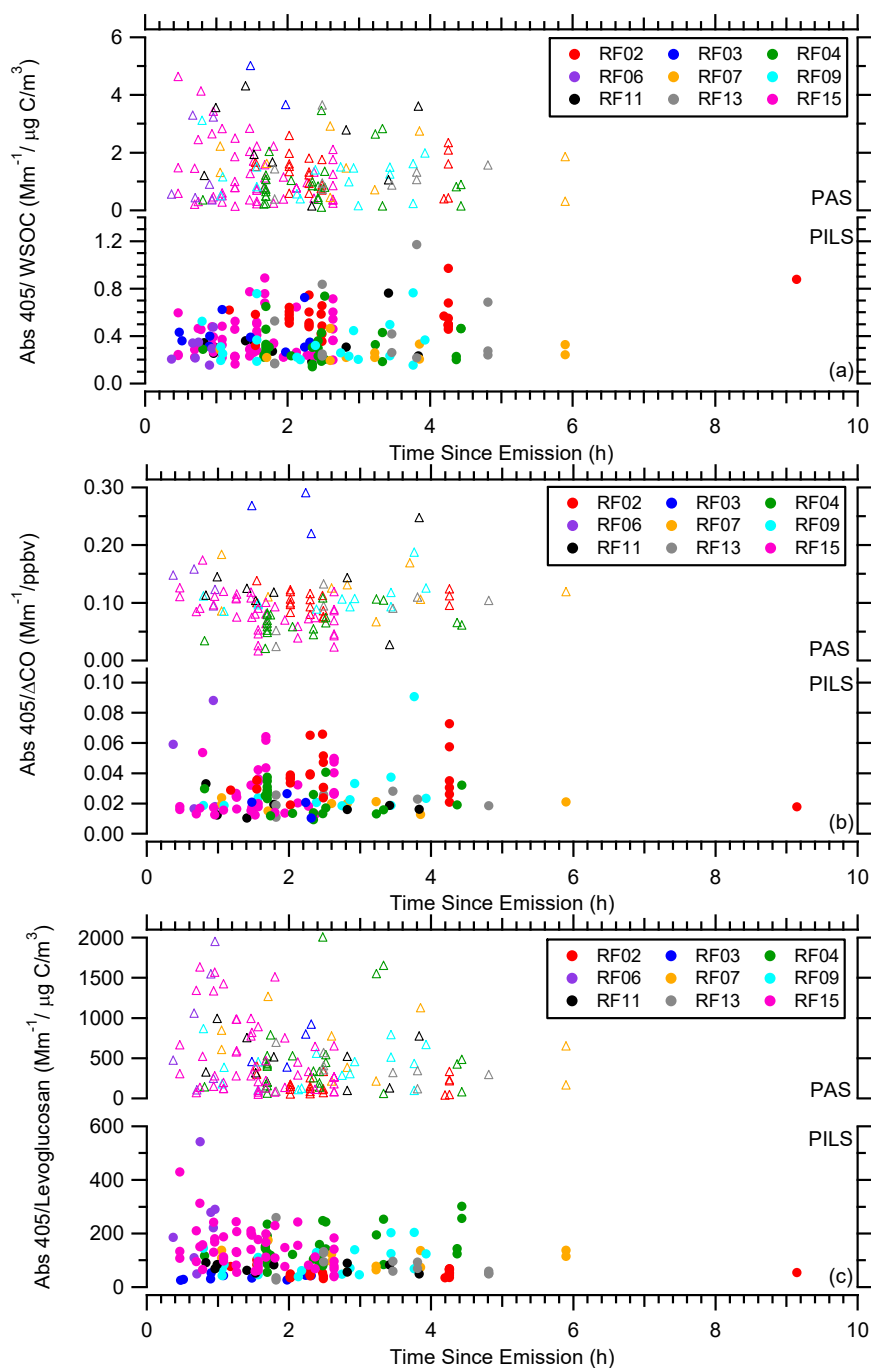


Figure 10. (a) Abs 405/WSOC, (b) Abs 405/ΔCO, and (c) Abs 405/levoglucosan as a function of time since emission for all WE-CAN flights with the data segregated by flight. In each plot the PAS total Abs 405 BrC is on top and the PILS water-soluble Abs 405 on the bottom.



491 (Figure 11 and Figures S4-S6), except that an overall lower Abs 405/levoglucosan ratio was  
492 observed for the wildfires with higher MCE values (i.e., Flight RF02). This further supports the  
493 relationship between the highest potassium concentrations and the levoglucosan vs. Abs 405  
494 correlation (Figures 8c and 8d) previously discussed as potassium is predominately emitted from  
495 the flaming phase of a fire [Echalar *et al.*, 1995; Lee *et al.*, 2010; Ward *et al.*, 1991].  
496

#### 497 **4. Summary**

498 A PILS-LWCC-TOC and PAS were deployed on the NSF/NCAR C-130 research aircraft  
499 during WE-CAN to examine aerosol absorption in wildfire smoke in the western U.S. This was  
500 the first deployment of the PILS-LWCC-TOC on a research aircraft. The PILS allowed for a 16  
501 s integrated measurement of the water-soluble BrC absorption and 4 s integrated measurement of  
502 WSOC. The data from the PILS and PAS were combined to investigate the water-soluble vs.  
503 total BrC absorption at 405 nm in the 20 wildfires sampled during WE-CAN. We show the  
504 following:  
505

- 506 1. WSOC, PILS water-soluble Abs 405, and PAS total Abs 405 BrC tracked each other in  
507 and out of the smoke plumes. BrC absorption was correlated with CO ( $R^2$  value for PAS  
508 = 0.76 and PILS = 0.55) and WSOC ( $R^2$  value for PAS = 0.42 and PILS = 0.60) during  
509 the entire study, illustrating the importance of biomass burning as a source of BrC  
510 absorption. A similar pattern was observed for levoglucosan, but with two data branches.  
511 Levoglucosan and BrC absorption were correlated ( $R^2$  values for PAS = 0.60 and PILS =  
512 0.76) in the first data branch and this subset of data was also characterized by the highest  
513 observed water-soluble potassium concentrations ( $> 0.5 \mu\text{g}/\text{m}^3$ ). This suggests there may  
514 be a relationship between levoglucosan and water-soluble potassium in wildfire  
515 emissions that has not generally been observed in other types of burning.  
516
- 517 2. Using the calculated UHSAS mass, the PILS water-soluble Abs 405 can be corrected to  
518 also account for the non-water-soluble fraction of the aerosol. The corrected PILS water-  
519 soluble Abs 405 showed good closure with the PAS total Abs 405 BrC, but with a factor  
520 of ~1.5 to 2 difference. This difference can be explained by particle vs. bulk solution  
521 absorption measured by the PAS vs. PILS, respectively, as shown by Mie Theory  
522 calculations. During WE-CAN, ~45% of the BrC absorption was due to water-soluble  
523 species.  
524
- 525 3. The ratio of water-soluble BrC absorption to WSOC,  $\Delta\text{CO}$ , or levoglucosan showed no  
526 clear dependence on fire dynamics or the time since emission up to 9 h. The total BrC  
527 absorption did show a slight decrease in the first 2 h, suggesting a need to further explore  
528 near source evolution.  
529

530  
531  
532  
533  
534  
535  
536

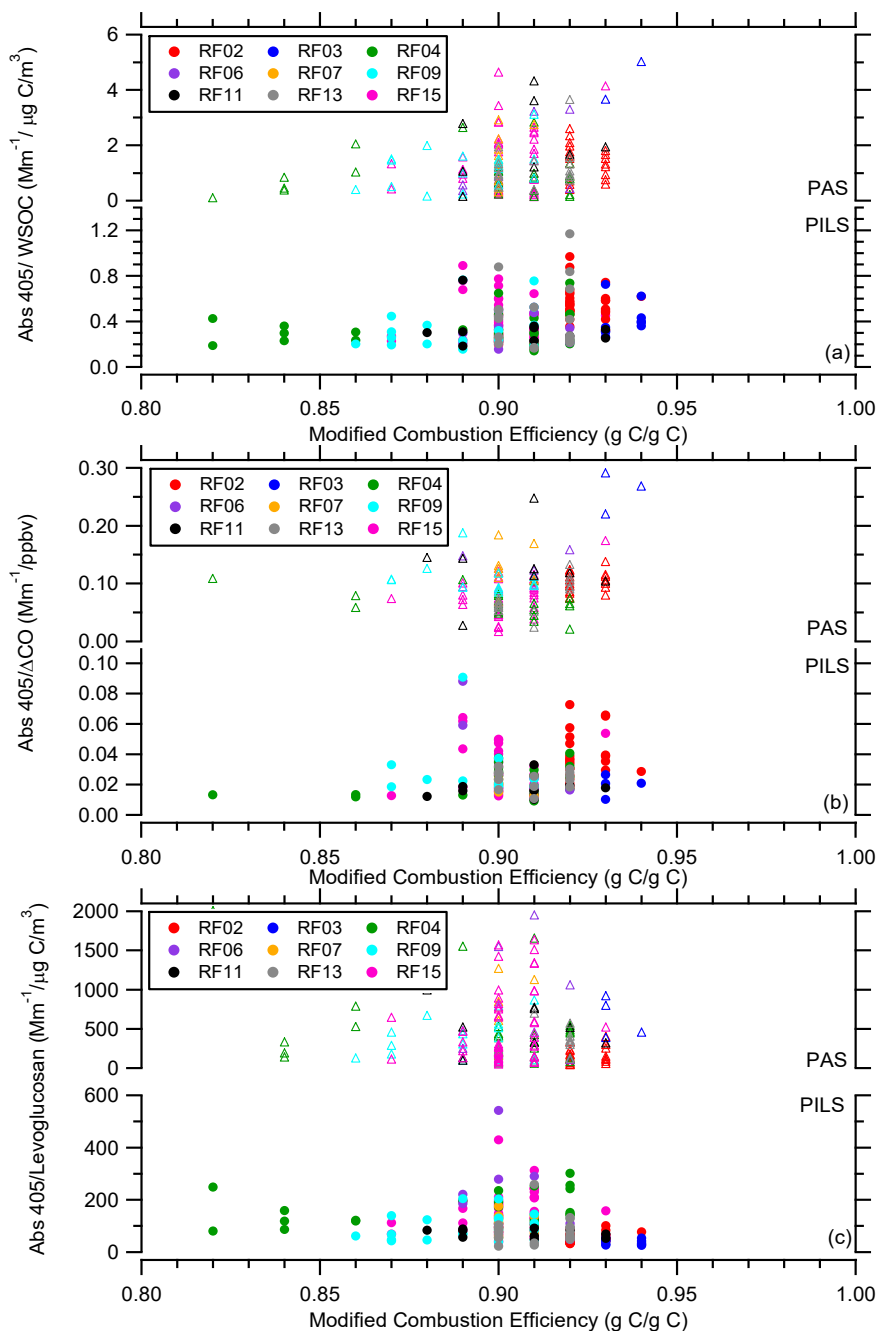


Figure 11. (a) Abs 405/WSOC, (b) Abs 405/ $\Delta$ CO, and (c) Abs 405/levoglucosan as a function of modified combustion efficiency for all WE-CAN flights with the data segregated by flight. In each plot the PAS total Abs 405 BrC is on top and the PILS water-soluble Abs 405 on the bottom.



537 **Data Availability**

538 The WE-CAN data is provided by NCAR/EOL under sponsorship of the National Science  
539 Foundation and is available at [http://data.eol.ucar.edu/master\\_lists/generated/we-can/](http://data.eol.ucar.edu/master_lists/generated/we-can/). The DOI  
540 for each data set used in this work are:

541  
542 PILS1: <https://doi.org/10.26023/9H07-MD9K-430D> and [https://doi.org/10.26023/CRHY-NDT9-](https://doi.org/10.26023/CRHY-NDT9-C30V)  
543 C30V

544 PILS2: <https://doi.org/10.26023/7TAN-TZMD-680Y>

545 PAS: <https://doi.org/10.26023/K8P0-X4T3-TN06>

546 UHSAS: <https://doi.org/10.26023/BZ4F-EAC4-290W>

547 CO: <https://doi.org/10.26023/NNYM-Z18J-PX0Q>

548 Meteorological Data and Coordinates: <https://doi.org/10.26023/G766-BS71-9V03>

549

550 **Author Contributions**

551 APS, SMM, DWT, EVF, JLC designed the project. APS wrote the paper. APS, RPP, YS,  
552 SMM, DWT, TC, JL, and EVF collected and analyzed data. All authors reviewed and provided  
553 comments for the paper.

554

555 **Conflict of Interest**

556 The authors declare that they have no conflict of interest.

557

558 **Acknowledgements**

559 We wish to thank RAF personnel for their many contributions supporting the field deployment.  
560 We also thank R.J. Weber for generously providing some of the parts used in the PILS racks.

561

562 **Financial Support**

563 This work was supported by the National Science Foundation under AGS-1650786.

564

565

566

567

568

569

570

571

572

573

574

575

576

577

578

579

580

581

582



583 **References**

- 584 Andreae, M.O. and A. Gelencsér, Black carbon or brown carbon? The nature of light-absorbing  
585 carbonaceous aerosols, *Atmos. Chem. Phys.*, *6*, 3131-3148, doi:10.5194/acp-6-3131-  
586 2006, 2006.  
587
- 588 Arnott, W.P., H. Moosmüller, C.F. Rogers, T. Jin, and R. Bruch, Photoacoustic spectrometer for  
589 measuring light absorption by aerosol: instrument description, *Atmos. Environ.*, *33*, 2845-  
590 2852, 1999.  
591
- 592 Chakrabarty, R.K., H. Moosmüller, L.-W. A. Chen, K. Lewis, W.P. Arnott, C. Mazzoleni, M.K.  
593 Dubey, C.E. Wold, W.M. Hao, and S.M. Kreidenweis, Brown carbon in tar balls from  
594 smoldering biomass combustion, *Atmos. Chem. Phys.*, *10*, 6363-6370, doi:10.5194/acp-  
595 10-6363-2010, 2010.  
596
- 597 Craig, L., A. Moharreri, D. C. Rogers, B. Anderson, and S. Dhaniyala, Aircraft-Based Aerosol  
598 Sampling in Clouds: Performance Characterization of Flow-Restriction Aerosol Inlets,  
599 *Journal of Atmospheric and Oceanic Technology*, *31*, 2512-2521, doi:10.1175/jtech-d-  
600 14-00022.1, 2014.  
601
- 602 Craig, L., A. Moharreri, A. Schanot, D. C. Rogers, B. Anderson, and S. Dhaniyala,  
603 Characterizations of Cloud Droplet Shatter Artifacts in Two Airborne Aerosol Inlets,  
604 *Aerosol Science and Technology*, *47*, 662-671, doi:10.1080/02786826.2013.780648,  
605 2013a.  
606
- 607 Craig, L., A. Schanot, A. Moharreri, D. C. Rogers, and S. Dhaniyala, Design and Sampling  
608 Characteristics of a New Airborne Aerosol Inlet for Aerosol Measurements in Clouds,  
609 *Journal of Atmospheric and Oceanic Technology*, *30*, 1123-1135, doi:10.1175/jtech-d-  
610 12-00168.1, 2013b.  
611
- 612 Desyaterik, Y., Y. Sun, X. Shen, T. Lee, X. Wang, T. Wang, and J.L. Collett Jr., Speciation of  
613 “brown” carbon in cloud water impacted by agricultural biomass burning in eastern  
614 China, *J. Geophys. Res.*, *118*, 7389-7399, doi:10.1022/jgrd.50561, 2013.  
615
- 616 Duarte, R.M.B.O., C.A. Pio, and A.C. Duarte, Spectroscopic study of the water-soluble organic  
617 matter isolated from atmospheric aerosols collected under different atmospheric  
618 conditions, *Analytica Chimica Acta*, *530*, 7-14, 2005.  
619
- 620 Duarte, R.M.B.O., M. Piñeiro-Iglesias, P. López-Mahía, S. Muniategui-Lorenzo, J. Moreda-  
621 Piñeiro, A.M.S. Silva, and A.C. Duarte, Comparative study of atmospheric water-soluble  
622 organic aerosols composition in contrasting suburban environments in the Iberian  
623 Peninsula Coast, *Science of the Total Environment*, *648*, 430-441, 2019.  
624
- 625 Eatough, D.J., A. Wadsworth, D.A. Eatough, J.W. Crawford, L.D. Hansen, and E.A. Lewis, A  
626 multiple system, multi-channel diffusion denuder sampler for the determination of fine-  
627 particulate organic material in the atmosphere, *Atmos. Environ.*, *27A*, 1213-1219, 1993.  
628



- 629 Echalar, F., A. Gaudichet, H. Cachier, and P. Artaxo, Aerosol emissions by tropical forest and  
630 savanna biomass burning: Characteristic trace elements and fluxes, *Geophys. Res. Lett.*,  
631 22, 3039-3042, 1995.  
632
- 633 Feng, Y., V. Ramanathan, and V.R. Kotamarthi, Brown carbon: a significant atmospheric  
634 absorber of solar radiation?, *Atmos. Chem. Phys.*, 13, 8607-8621, doi:10.5194/acp-13-  
635 8607-2013, 2013.  
636
- 637 Forrister, H., J. Liu, E. Scheuer, J. Dibb, L. Ziemba, K.L. Thornhill, B. Anderson, G. Diskin,  
638 A.E. Perring, J.P. Schwarz, P. Campuzano-Jost, D.A. Day, B.B. Palm, J.L. Jimenez, A.  
639 Nenes, and R.J. Weber, Evolution of brown carbon in wildfire plumes, *Geophys. Res.*  
640 *Lett.*, 42, 4623-4630, doi:10.1002/2015GL063897, 2015.  
641
- 642 Foster, K., R. Pokhrel, M. Burkhardt, and S. Murphy, A novel approach to calibrating a  
643 photoacoustic absorption spectrometer using polydisperse absorbing aerosol, *Atmos.*  
644 *Meas. Tech.*, 12, 3351-3363, doi:10.5194/amt-12-3351-2019, 2019.  
645
- 646 Gerbig, C., S. Schmitgen, D. Kley, A. Volz-Thomas, K. Dewey, and D. Haaks, An improved  
647 fast-response vacuum-UV resonance fluorescence CO instrument, *J. Geophys. Res.*, 104,  
648 1699-1704, 1999.  
649
- 650 Hecobian, A., X. Zhang, M. Zheng, N.H. Frank, E.S. Edgerton, and R.J. Weber, Water-soluble  
651 organic aerosol material and the light-absorption characteristics of aqueous extracts  
652 measured over the Southeastern United States, *Atmos. Chem. Phys.*, 10, 5965-5977,  
653 doi:10.5194/acp-10-5965-2010, 2010.  
654
- 655 Hems, R.F. and J.P.D. Abbatt, Aqueous Phase Photo-oxidation of Brown Carbon Nitrophenols:  
656 Reaction Kinetics, Mechanism, and Evolution of Light Absorption, *ACS Earth Space*  
657 *Chem.*, 2, 225-234, doi:10.1021/acsearthspacechem.7b00123, 2018.  
658
- 659 Hoffer, A., A. Gelencsér, P. Guyon, G. Kiss, O. Schmid, G.P. Frank, P. Artaxo, and M.O.  
660 Andreae, Optical properties of humic-like substance (HULIS) in biomass-burning  
661 aerosols, *Atmos. Chem. Phys.*, 6, 3563-3570, doi:10.5194/acp-6-3563-2006, 2006.  
662
- 663 Jacobson, M.C., H.-C. Hansson, K.J. Noone, and R.J. Charlson, Organic atmospheric aerosols:  
664 Review and state of the science, *Rev. Geophys.*, 38, 267-294, 2000.  
665
- 666 Jo, D.S., R.J. Park, S. Lee, S.-W. Kim, and X. Zhang, A global simulation of brown carbon:  
667 implications for photochemistry and direct radiative effect, *Atmos. Chem. Phys.*, 16,  
668 3413-3432, doi:10.5194/acp-16-3413-2016, 2016.  
669
- 670 Kanakidou, M., et al., Organic aerosol and global climate modelling: a review, *Atmos. Chem.*  
671 *Phys.*, 5, 1053-1123, doi:10.5194/acp-5-1053-2005, 2005.  
672
- 673 Kirchstetter, T.W. and T.L. Thatcher, Contribution of organic carbon to wood smoke particulate  
674 matter absorption of solar radiation, *Atmos. Chem. Phys.*, 12, 6067-6072,





- 675 doi:10.5194/acp-12-6067-2012, 2012.  
676  
677 Kirchstetter, T.W., T. Novakov, and P.V. Hobbs, Evidence that the spectral dependence of light  
678 absorption by aerosols is affected by organic carbon, *J. Geophys. Res.*, *109*, D21208,  
679 doi:10.1029/2004JD004999, 2004.  
680  
681 Lack, D.A. and J.M. Langridge, On the attribution of black and brown carbon light absorption  
682 using the Ångström exponent, *Atmos. Chem. Phys.*, *13*, 10535-10543, doi:10.5194/acp-  
683 13-10535-2013, 2013.  
684  
685 Lack, D.A., J.M. Langridge, R. Bahreini, C.A. Brock, A.M. Middlebrook, and J.P. Schwarz,  
686 Brown Carbon and Internal Mixing in Biomass Burning Particles, *P. Natl. Acad. Sci.*,  
687 *109*, 14802-14807, doi:10.1073/pnas.1206575109, 2012.  
688  
689 Langridge, J.M., M.S. Richardson, D.A. Lack, C.A. Brock, and D.M. Murphy, Limitations of the  
690 Photoacoustic Technique for Aerosol Absorption Measurement at High Relative  
691 Humidity, *Aerosol Sci. Technol.*, *47*, 1163-1173, doi:10.1080/02786826.2013.827324,  
692 2013.  
693  
694 Lee, T., A.P. Sullivan, L. Mack, J.L. Jimenez, S.M. Kreidenweis, T.B. Onasch, D.R. Worsnop,  
695 W. Malm, C.E. Wold, W.M. Hao, and J.L. Collett, Jr., Chemical smoke marker emissions  
696 during flaming and smoldering phases of laboratory open burning of wildland fuels,  
697 *Aerosol Res. Lett.*, *44*, i-v, 2010.  
698  
699 Limbeck, A., M. Kulmala, and H. Puxbaum, Secondary organic aerosol formation in the  
700 atmosphere via heterogeneous reaction of gaseous isoprene on acidic particles, *Geophys.*  
701 *Res. Lett.*, *30*(19), 1996, doi: 10.1029/2003GL017738, 2003.  
702  
703 Liu, J., M. Bergin, H. Guo, L. King, N. Kotra, E. Edgerton, and R.J. Weber, Size-resolved  
704 measurements of brown carbon in water and methanol extracts and estimates of their  
705 contribution to ambient fine-particle light absorption, *Atmos. Chem. Phys.*, *13*, 12389-  
706 12404, doi:10.5194/acp-13-12389-2013, 2013.  
707  
708 Liu, J., E. Scheuer, J. Dibb, G.S. Diskin, L.D. Ziemba, K.L. Thornhill, B.E. Anderson, A.  
709 Wisthaler, T. Mikoviny, J.J. Devi, M. Bergin, A.E. Perring, M.Z. Markovic, J.P.  
710 Schwarz, P. Campuzano-Jost, D.A. Day, J.L. Jimenez, and R.J. Weber, Brown carbon  
711 aerosol in the North American continental troposphere: sources, abundances, and  
712 radiative forcing, *Atmos. Chem. Phys.*, *15*, 7841-7858, doi:10.5194/acp-15-7841-2015,  
713 2015.  
714  
715 Liu, J., E. Scheuer, J. Dibb, L.D. Ziemba, K.L. Thornhill, B.E. Anderson, A. Wisthaler, T.  
716 Mikoviny, J.J. Devi, M. Bergin, and R.J. Weber, Brown carbon in the continental  
717 troposphere, *Geophys. Res. Lett.*, *41*, 2191-2195, doi:10.1002/2013GL058976, 2014.  
718  
719 Lukács, H., A. Gelencsér, S. Hammer, H. Puxbaum, C. Pio, M. Legrand, A. Kasper-Giebl, M.  
720 Handler, A. Limbeck, D. Simson, S. Preunkert, Seasonal trends and possible sources of



- 721 brown carbon based on 2-year aerosol measurements at six sites in Europe, *J. Geophys.*  
722 *Res.*, *112*, D23S18, doi:10.1029/2006JD008151, 2007.
- 723
- 724 Marple, V.A., K.L. Rubow, and S.M. Behm, A microorifice uniform deposit impactor (MOUDI):  
725 description, calibration, and use, *Aerosol Sci. Technol.*, *14*, 434-446, 1991.
- 726
- 727 Moharreri, A., L. Craig, P. Dubey, D. C. Rogers, and S. Dhaniyala, Aircraft testing of the new  
728 Blunt-body Aerosol Sampler (BASE), *Atmospheric Measurement Techniques*, *7*, 3085-  
729 3093, doi:10.5194/amt-7-3085-2014, 2014.
- 730
- 731 Mohr, C., F.D. Lopez-Hilfiker, P. Zotter, A.S.H. Prévôt, L. Xu, N.L. Ng, S.C. Herndon, L.R.  
732 Williams, J.P. Franklin, M.S. Zahniser, D.R. Worsnop, W.B. Knighton, A.C. Aiken, K.J.  
733 Gorkowski, M.K. Dubey, J.D. Allan, and J.A. Thornton, Contribution of Nitrated Phenols  
734 to Wood Burning Brown Carbon Light Absorption in Detling, United Kingdom during  
735 Winter Time, *Environ. Sci. Technol.*, *47*, 6316-6324, 2013.
- 736
- 737 Moosmüller, H., R.K. Chakrabarty, W.P. Arnott, Aerosol light absorption and its measurement:  
738 A review, *J. Quant. Spectrosc. Radiat. Transfer*, *110*, 844-878,  
739 doi:10.1016/j.jqsrt.2009.02.035, 2009.
- 740
- 741 Orsini, D.A., Y. Ma, A. Sullivan, B. Sierau, K. Baumann, and R.J. Weber, Refinements to the  
742 particle-into-liquid sampler (PILS) for ground and airborne measurements of water-  
743 soluble aerosol composition, *Atmos. Environ.*, *37*, 1243-1259, 2003.
- 744
- 745 Pokhrel, R.P., E.R. Beamesderfer, N.L. Wagner, J.M. Langridge, D.A. Lack, T. Jayarathne, E.A.  
746 Stone, C.E. Stockwell, R.J. Yokelson, and S.M. Murphy, Relative importance of black  
747 carbon, brown carbon, and absorption enhancement from clear coatings in biomass  
748 burning emissions, *Atmos. Chem. Phys.*, *17*, 5063-5078, doi:10.5194/acp-17-5063-2017,  
749 2017.
- 750
- 751 Saleh, R., C.J. Hennigan, G.R. McMeeking, W.K. Chuang, E.S. Robinson, H. Coe, N.M.  
752 Donahue, and A.L. Robinson, Absorptivity of brown carbon in fresh and photo-  
753 chemically aged biomass-burning emissions, *Atmos. Chem. Phys.*, *13*, 7683-7693,  
754 doi:10.5194/acp-13-7683-2013, 2013.
- 755
- 756 Sareen, N., A.N. Schwier, E.L. Shapiro, D. Mitroo, and V.F. McNeill, Secondary organic  
757 material formed by methylglyoxal in aqueous aerosol mimics, *Atmos. Chem. Phys.*, *10*,  
758 997-1016, doi:10.5194/acp-10-977-2010, 2010.
- 759
- 760 Saxena, P. and L.M. Hildemann, Water-soluble organics in atmospheric particles: A critical  
761 review of the literature and applications of thermodynamics to identify candidate  
762 compounds, *J. Atmos. Chem.*, *24*, 57-109, 1996.
- 763
- 764 Schauer, J.J., M.J. Kleeman, G.R. Cass, and B.R.T. Simoneit, Measurement of Emissions from  
765 Air Pollution Sources. 3. C<sub>1</sub>-C<sub>29</sub> Organic Compounds from Fireplace Combustion of  
766 Wood, *Environ. Sci. Technol.*, *35*, 1716-1728, 2001.



- 767  
768 Simoneit, B.R.T., J.J. Schauer, C.G. Nolte, D.R. Oros, V.O. Elias, M.P. Fraser, W.F. Rogge, and  
769 G.R. Cass, Levoglucosan, a tracer for cellulose in biomass burning and atmospheric  
770 particles, *Atmos. Environ.*, *33*, 173-182, 1999.  
771  
772 Sorooshian, A., F.J. Brechtel, Y. Ma, R.J. Weber, A. Corless, R.C. Flagan, and J.H. Seinfeld,  
773 Modeling and Characterization of a Particle-into-Liquid Sampler (PILS), *Aerosol Sci.*  
774 *Technol.*, *40*, 396-409, 2006.  
775  
776 Sullivan, A.P., H. Guo, J.C. Schroder, P. Campuzano-Jost, J.L. Jimenez, T. Campos, V. Shah, L.  
777 Jaeglé, B.H. Lee, F.D. Lopez-Hilfiker, J.A. Thornton, S.S. Brown, and R.J. Weber,  
778 Biomass Burning Markers and Residential Burning in the WINTER Aircraft Campaign,  
779 *J. Geophys. Res.*, *124*, doi:10.1029/2017JD028153, 2019.  
780  
781 Sullivan, A.P., N. Frank, D.M. Kenski, and J.L. Collett Jr., Application of High-Performance  
782 Anion-Exchange Chromatography – Pulsed Amperometric Detection for Measuring  
783 Carbohydrates in Routine Daily Filter Samples Collected by a National Network: 2.  
784 Examination of Sugar Alcohols/Polyols, Sugars, and Anhydrosugars in the Upper  
785 Midwest, *J. Geophys. Res.*, *116*, D08303, doi:10.1029/2010JD014169, 2011b.  
786  
787 Sullivan, A.P., N. Frank, G. Onstad, C.D. Simpson, and J.L. Collett, Jr., Application of High-  
788 Performance Anion-Exchange Chromatography – Pulsed Amperometric Detection for  
789 Measuring Carbohydrates in Routine Daily Filter Samples Collected by a National  
790 Network: 1. Determination of the Impact of Biomass Burning in the Upper Midwest, *J.*  
791 *Geophys. Res.*, *116*, D08302, doi:10.1029/2010JD014166, 2011a.  
792  
793 Sullivan, A.P., A.A. May, T. Lee, G.R. McMeeking, S.M. Kreidenweis, S.K. Akagi, R.J.  
794 Yokelson, S.P. Urbanski, and J.L. Collett, Jr., Airborne-Based Source Smoke Marker  
795 Ratios from Prescribed Burning, *Atmos. Chem. Phys.*, *14*, 10535-10545, doi:10.5194/acp-  
796 14-10535-2014, 2014.  
797  
798 Sumlin, B.J., A. Pandey, M.J. Walker, R.S. Pattison, B.J. Williams, and R.K. Chakrabarty,  
799 Atmospheric Photooxidation Diminishes Light Absorption by Primary Brown Carbon  
800 Aerosol from Biomass Burning, *Environ. Sci. Technol. Lett.*, *4*, 540-545,  
801 doi:10.1021/acs/estlett.7b00393, 2017.  
802  
803 Updyke, K.M., T.B. Nguyen, and S.A. Nizkorodov, Formation of brown carbon via reactions of  
804 ammonia with secondary organic aerosols from biogenic and anthropogenic precursors,  
805 *Atmos. Environ.*, *63*, 22-31, 2012.  
806  
807 Verma, V., Y. Wang, R. El-Afifi, T. Fang, J. Rowland, A.G. Russell, and R.J. Weber,  
808 Fractionating ambient humic-like substances (HULIS) for their reactive oxygen species  
809 activity – Assessing the importance of quinones and atmospheric aging, *Atmos. Environ.*,  
810 *120*, 351-359, 2015.  
811  
812 Ward, D.E. and L.F. Radke, Emission measurements from vegetation fires: a comparative



- 813 evaluation of methods and results, in *Fire in the environment: the ecological,*  
814 *atmospheric, and climatic importance of vegetation fires*, edited by P.J. Crutzen and J.G.  
815 Goldammer, pp. 53-76, Wiley, Chichester, England, 1993.  
816
- 817 Ward, D.E., A.W. Setzer, Y.J. Kaufman, and R.A. Rasmussen, Characteristics of smoke  
818 emissions from biomass fires of the Amazon region-BASE-A experiment, in *Global*  
819 *Biomass Burning: Atmospheric, Climatic, and Biospheric Implications*, edited by J.S.  
820 Levine, pp. 394-402, MIT Press, Cambridge, MA, 1991.  
821
- 822 Wong, J.P.S., M. Tsagkaraki, I. Tsiodra, N. Mihalopoulos, K. Violaki, M. Kanakidou, J.  
823 Sciare, A. Nenes, and R.J. Weber, Atmospheric evolution of molecular-weight-  
824 separated brown carbon from biomass burning, *Atmos. Chem. Phys.*, *19*, 7319-7334,  
825 doi:10.5194/acp-19-7319-2019, 2019.  
826
- 827 Yttri, K.E., W. Aas, A. Bjerke, J.N. Cape, F. Cavalli, D. Ceburnis, C. Dye, L. Emblico, M.C.  
828 Facchini, C. Forster, J.E. Hanssen, H.C. Hansson, S.G. Jennings, W. Maenhaut, J.P.  
829 Putaud, and K. Tørseth, Elemental and organic carbon in PM<sub>10</sub>: a one year  
830 measurement campaign within the European Monitoring and Evaluation Programme  
831 EMEP, *Atmos. Chem. Phys.*, *7*, 5711-5725, 2007.  
832
- 833 Zeng, L., J. Dibb, E. Scheuer, J.M. Katich, J.P. Schwarz, I. Bourgeois, J. Peischl, T. Ryerson,  
834 C. Warneke, A.E. Perring, G.S. Diskin, J.P. DiGangi, J.B. Nowak, R.H. Moore, E.B.  
835 Wiggins, D. Pagonis, H. Guo, P. Campuzano-Jost, J.L. Jimenez, L. Xu, and R. J.  
836 Weber, Characteristics and Evolution of Brown Carbon in Western United States  
837 Wildfires, *Atmos. Chem. Phys. Discuss. [preprint]*, doi:10.5194/acp-2022-70, in  
838 review, 2022.  
839
- 840 Zeng, L., A. Zhang, Y. Wang, N.L. Wagner, J.M. Katich, J.P. Schwarz, G.P. Schill, C.  
841 Brock, K.D. Froyd, D.M. Murphy, C.J. Williamson, A. Kupac, E. Scheuer, J. Dibb,  
842 and R.J. Weber, Global Measurements of Brown Carbon and Estimated Direct  
843 Radiative Effects, *Geophys. Res. Lett.*, *47*, e2020GL088747,  
844 doi:10.1029/2020GL088747, 2020.  
845
- 846 Zhang, A., Y. Wang, Y. Zhang, R.J. Weber, Y. Song, Z. Ke, and Y. Zou, Modeling the  
847 global radiative effect of brown carbon: a potentially larger heating source in the  
848 tropical free troposphere than black carbon, *Atmos. Chem. Phys.*, *20*, 1901-1920,  
849 doi:10.5194/acp-20-1901-2020, 2020.  
850
- 851 Zhang, Q., et al., Ubiquity and dominance of oxygenated species in organic aerosols in  
852 anthropogenically-influenced Northern Hemisphere midlatitudes, *Geophys. Res. Lett.*,  
853 *34*, L13801, doi:10.1029/GL029979, 2007.  
854
- 855 Zhang, X., Y.-H. Lin, J.D. Surratt, and R.J. Weber, Sources, Composition and Absorption  
856 Ångström Exponent of Light-absorbing Organic Components in Aerosol Extracts  
857 from the Los Angeles Basin, *Environ. Sci. Technol.*, *47*, 3685-3693,  
858 doi:10.1021/es305047b, 2013.



- 859  
860 Zhang, X., Y.-H. Lin, J.D. Surratt, P. Zotter, A.S.H. Prévôt, and R.J. Weber, Light-absorbing  
861 soluble organic aerosol in Los Angeles and Atlanta: A contrast in secondary organic  
862 aerosol, *Geophys. Res. Lett.*, 38, L21810, doi:10.1029/2011GL049385, 2011.  
863  
864 Zhang, Y., H. Forrister, J. Liu, J. Dibb, B. Anderson, J.P. Schwarz, A.E. Perring, J.L.  
865 Jimenez, P. Campuzano-Jost, Y. Wang, A. Nenes, and R.J. Weber, Top-of-  
866 atmosphere radiative forcing affected by brown carbon in the upper troposphere,  
867 *Nature Geoscience*, 10, 486-489, doi:10.1038/NGEO2960, 2017.  
868  
869 Zhao, R., A.K.Y. Lee, L. Huang, X. Li., F. Yang, and J.P.D. Abbatt, Photochemical  
870 processing of aqueous atmospheric brown carbon, *Atmos. Chem. Phys.*, 15, 6087-  
871 6100, doi:10.5194/acp-15-6087-2015, 2015.  
872  
873 Zhong, M. and M. Jang, Dynamic light absorption of biomass-burning organic carbon  
874 photochemically aged under natural sunlight, *Atmos. Chem. Phys.*, 14, 1517-1525,  
875 doi:10.5194/acp-14-1517-2014, 2014.  
876